Supporting Information for:

Enhancement for phonon-mediated superconductivity up to 37 K in few-hydrogen metal-bonded layered magnesium hydride under atmospheric pressure

Yong He,[1] Juan Du,[2,*] Shi-ming Liu,[1] Chong Tian,[1] Min Zhang,[3]
Yao-hui Zhu,[4] Hongxia Zhong,[5] Xinqiang Wang,[1] and Jun-jie Shi[1,†]

[1] *State Key Laboratory for Artificial Microstructures and Mesoscopic Physics, School of Physics, Peking University Yangtze Delta Institute of Optoelectronics, Peking University, Beijing 100871, China*
[2] *Department of Physics and Optoelectronic Engineering Faculty of Science, Beijing University of Technology, Beijing 100124, China*
[3] *Inner Mongolia Key Laboratory for Physics and Chemistry of Functional Materials, College of Physics and Electronic Information, Inner Mongolia Normal University, Hohhot 010022, China*
[4] *Physics Department, Beijing Technology and Business University, Beijing 100048, China*
[5] *School of Mathematics and Physics, China University of Geosciences, Wuhan 430074, China*

COMPUTATIONAL METHODS

The structural optimization and electronic characteristics of few-hydrogen metal-bonded layered $(Mg_4)_2H_1$ are explored based on the density functional theory (DFT) method, employing the QUANTUM ESPRESSO package [1–3]. To obtain optimal lattice constants, the generalized gradient approximation (GGA) of the revised Perdew-Burke-Ernzerhof (PBEsol) functional is employed to treat the exchange-correlation (XC) interactions [4]. subsequently, the GGA of Perdew-Burke-Ernzerhof (PBE) functional is adopted in electronic structure calculations [5]. The interactions between core electrons and valence electrons are described by the Optimized Norm-Conserving Vanderbilt (ONCV) pseudopotential, with the valence electron configurations as $2s^2 2p^6 3s^2$ for Mg and $1s^1$ for H atoms [6]. The kinetic energy cutoff for plane wave and charge density is set to 120 and 480 Ry, respectively. The structure is fully optimized until the force on each atom is less than 10^{-5} Ry/Bohr. The self-consistent charge density is evaluated using an 8×8×10 k-point grid with a Gaussian smearing of 0.01 Ry. Phonon wave vectors are sampled on a 4×4×5 mesh.

The dynamical matrices and electron-phonon coupling (EPC) are computed within the framework of density functional perturbation theory (DFPT) [7]. The EPC matrix element $g^{ij}_{\mathbf{k},\mathbf{q}\nu}$ is used to describe the scattering probability amplitude of an electron by a phonon with wave vector $\mathbf{q}$, which can be determined as follows [8, 9],

$$g^{ij}_{\mathbf{k},\mathbf{q}\nu} = \left(\frac{\hbar}{2M\omega_{\mathbf{q}\nu}}\right)^{1/2} \left\langle \psi_{i,\mathbf{k}} \middle| \frac{dV_{\mathrm{SCF}}}{d\hat{u}_{\mathbf{q}\nu}} \cdot \hat{e}_{\mathbf{q}\nu} \middle| \psi_{j,\mathbf{k}+\mathbf{q}} \right\rangle, \tag{S1}$$

where M represents the atomic mass, $\mathbf{k}$ and $\mathbf{q}$ are electron and phonon wave vectors. The i, j and ν are indices of energy bands and phonon modes, respectively. The $\omega_{\mathbf{q}\nu}$ and $\hat{e}_{\mathbf{q}\nu}$ stand for the phonon frequency and eigenvector of the νth phonon mode with wave vector $\mathbf{q}$. The $dV_{\mathrm{SCF}}/d\hat{u}_{\mathbf{q}\nu}$ measures the change of self-consistent potential induced by the atomic displacement. Both $\psi_{i,\mathbf{k}}$ and $\psi_{j,\mathbf{k}+\mathbf{q}}$ are Kohn-Sham orbitals. Phonon linewidth $\gamma_{\mathbf{q}\nu}$ can be defined by the integration [8, 9],

$$\gamma_{\mathbf{q}\nu} = \frac{2\pi\omega_{\mathbf{q}\nu}}{\Omega_{\mathrm{BZ}}} \sum_{ij} \int d^3k |g^{ij}_{\mathbf{k},\mathbf{q}\nu}|^2 \delta\left(\epsilon_{\mathbf{k},i} - \epsilon_F\right) \delta\left(\epsilon_{\mathbf{k}+\mathbf{q},j} - \epsilon_F\right), \tag{S2}$$

where $\epsilon_{\mathbf{k},i}$ and $\epsilon_{\mathbf{k}+\mathbf{q},j}$ are eigenvalues of Kohn-Sham orbitals at given bands and wave vectors. It is clear that the phonon linewidth is mainly determined by the EPC matrix element and the Fermi surface (FS) nesting function $\xi(\mathbf{q})$,

* dujuan1121@bjut.edu.cn
† jjshi@pku.edu.cn

defined as follows,

$$\xi(\mathbf{q}) = \sum_{\mathbf{k},i,j} \delta\left(\epsilon_{\mathbf{k},i} - \epsilon_F\right) \delta\left(\epsilon_{\mathbf{k}+\mathbf{q},j} - \epsilon_F\right). \tag{S3}$$

The Eliashberg spectral function can be expressed by [8, 9],

$$\alpha^2F(\omega) = \frac{1}{2\pi N(E_\mathrm{F})} \sum_{\mathbf{q}\nu} \delta\left(\omega - \omega_{\mathbf{q}\nu}\right) \frac{\gamma_{\mathbf{q}\nu}}{\hbar\omega_{\mathbf{q}\nu}}, \tag{S4}$$

where $N(E_\mathrm{F})$ represents the density of states at Fermi level. The EPC constant λ can be determined through integration of the spectral function in frequency space or summation over the first Brillouin zone [8, 9],

$$\lambda = 2\int \frac{\alpha^2F(\omega)}{\omega} d\omega = \sum_{\mathbf{q}\nu} \lambda_{\mathbf{q}\nu}, \tag{S5}$$

where the EPC parameter $\lambda_{\mathbf{q}\nu}$ for the mode ν at wave vector $\mathbf{q}$ is defined by [8, 9],

$$\lambda_{\mathbf{q}\nu} = \frac{\gamma_{\mathbf{q}\nu}}{\pi\hbar N(E_\mathrm{F})\omega^2_{\mathbf{q}\nu}}. \tag{S6}$$

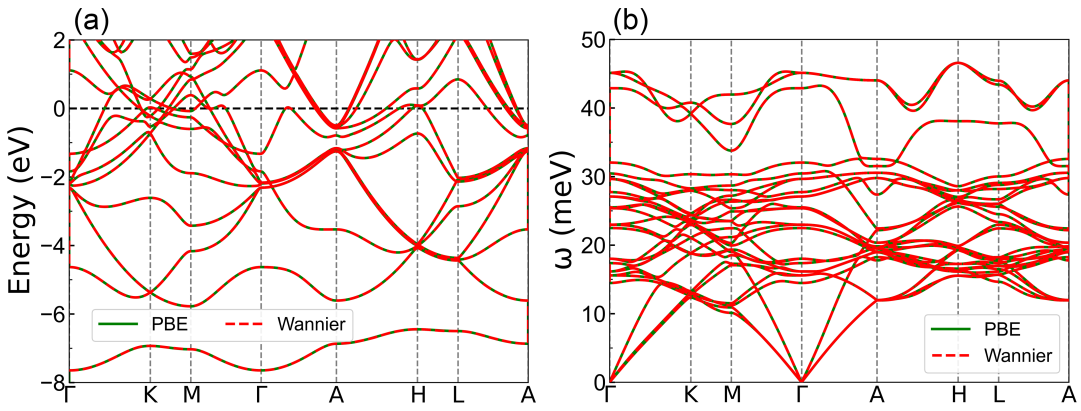

FIG. S1. Calculated (a) electronic band structures, and (b) phonon spectra of layered $(Mg_4)_2H_1$, where the green lines are derived from the first-principles PBE functional, and the red dashed lines are simulated by using the Wannier interpolation technology, respectively.

To further investigate the EPC property and the superconducting characteristics of layered $(Mg_4)_2H_1$, we adopt Wannier interpolation technique to reevaluate the EPC strength and solve the Migdal-Eliashberg (ME) equations [10, 11] by using the EPW code [12, 13]. The electronic wave functions are calculated using a dense k-point grid 8×8×10 within the EPW code, in order to perform the Wannier interpolation [12, 14]. The electronic properties near FS are described by constructing the maximally localized thirty-three Wannier functions [15]. The Wannier interpolated band structures and phonon spectra are shown in Fig. S1. The fully anisotropic ME equations can be described as follows [11],

$$\begin{aligned} Z\left(\mathbf{k}, i\omega_n\right) =& 1 + \frac{\pi T}{N(E_\mathrm{F})\omega_n} \sum_{\mathbf{k}'n'} \frac{\omega_{n'}}{\sqrt{\omega^2_{n'} + \Delta^2\left(\mathbf{k}', i\omega_{n'}\right)}} \\ & \times \delta\left(\epsilon_{\mathbf{k}'}\right) \lambda\left(\mathbf{k}, \mathbf{k}', n - n'\right), \end{aligned} \tag{S7}$$

$$\begin{aligned} Z\left(\mathbf{k}, i\omega_n\right) \Delta\left(\mathbf{k}, i\omega_n\right) =& \frac{\pi T}{N(E_\mathrm{F})} \sum_{\mathbf{k}'n'} \frac{\Delta\left(\mathbf{k}', i\omega_{n'}\right)}{\sqrt{\omega^2_{n'} + \Delta^2\left(\mathbf{k}', i\omega_{n'}\right)}} \\ & \times \delta\left(\epsilon_{\mathbf{k}'}\right) \left[\lambda\left(\mathbf{k}, \mathbf{k}', n - n'\right) - \mu^*\right]. \end{aligned} \tag{S8}$$

Here $Z(\mathbf{k}, i\omega_n)$ is the mass renormalization function and $\Delta(\mathbf{k}, i\omega_n)$ is the superconducting gap function. The $\mathbf{k}$ (n) is the electron wave vector (band index), and μ^* is the semiempirical Coulomb repulsion pseudopotential, which has

been set to 0.10 in our calculations. The anisotropic EPC strength $\lambda(\mathbf{k},\mathbf{k}',n-n')$ can be calculated by using the following formula,

$$\lambda\left(\mathbf{k},\mathbf{k}',n-n'\right)=N(E_{\mathrm{F}})\sum_{\nu}\frac{2\omega_{\mathbf{q}\nu}}{\left(\omega_{n}-\omega_{n'}\right)^{2}+\omega_{\mathbf{q}\nu}^{2}}|g_{\mathbf{k}\mathbf{k}'}^{\nu}|^{2}. \tag{S9}$$

It is worth emphasizing that the ME equations can only be solved self-consistently along the imaginary axis at the fermion Matsubara frequencies $\omega_n=(2n+1)\pi T$ (n an integer) for each temperature T because two equations are coupled with each other in a non-linear fashion. The numerical solutions of the ME equations for layered $(Mg_4)_2H_1$ are performed on the dense grids including 40×40×50 $\mathbf{k}$ points and 20×20×25 $\mathbf{q}$ points. The upper limit of Matsubara frequency is set to 10 times of the phonon cutoff frequency. The Dirac δ functions have been represented by Lorentzians of width 80 meV for electrons and 0.05 meV for phonons.

The specific heat of layered $(Mg_4)_2H_1$ is calculated from the free energy difference between the superconducting and normal states as follows [16, 17],

$$\begin{aligned}\Delta F=&-\pi T\sum_{n\mathbf{k}j}\left[\sqrt{\omega_{j}^{2}+\Delta_{n\mathbf{k}}^{2}\left(i\omega_{j}\right)}-|\omega_{j}|\right]\\&\times\left[Z_{n\mathbf{k}}\left(i\omega_{j}\right)-Z_{n\mathbf{k}}^{N}\left(i\omega_{j}\right)\frac{|\omega_{j}|}{\sqrt{\omega_{j}^{2}+\Delta_{n\mathbf{k}}^{2}\left(i\omega_{j}\right)}}\right]\\&\times\delta\left(\varepsilon_{n\mathbf{k}}-\varepsilon_{\mathrm{F}}\right).\end{aligned} \tag{S10}$$

Here, Z^N represents the mass renormalization function of the normal state N, calculated by setting Δ=0 in Eq. S7. The specific heat can be calculated from the second-order derivative of the free energy according to the following formula,

$$\Delta C(T)=-T\frac{d^{2}\Delta F}{dT^{2}}. \tag{S11}$$

The upper critical magnetic field $H_C(0)$ can be evaluated roughly by using the following equation under the condition of $T_c/\omega_{\log}$<0.25 [18],

$$\frac{\gamma T_{C}^{2}}{H_{C}^{2}(0)}=0.168\left[1-12.2\left(\frac{T_{C}}{\omega_{\log}}\right)^{2}\ln\left(\frac{\omega_{\log}}{3T_{C}}\right)\right], \tag{S12}$$

where T_c and $\omega_{\log}$ are critical temperature and logarithmic average phonon frequency, respectively. The Sommerfeld constant γ can be calculated from the following formula [18],

$$\gamma=\frac{2}{3}\pi^{2}k_{\mathrm{B}}^{2}N(0)(1+\lambda), \tag{S13}$$

where the $N(0)$=$N(E_{\mathrm{F}})/2$ is the density of states at Fermi level per spin.

STRUCTURAL PROPERTY

TABLE S1. The atomic positions of layered $(Mg_4)_2H_1$ with fractional coordinates.

Atom	x	y	z
Mg	0.833333313	0.666666687	0.248129994
Mg	0.166666687	0.333333313	0.751870036
Mg	0.333333313	0.166666627	0.248129994
Mg	0.666666687	0.833333373	0.751870036
Mg	0.833333373	0.166666687	0.248129994
Mg	0.166666627	0.833333313	0.751870036
Mg	0.666666687	0.333333343	0.746699989
Mg	0.333333313	0.666666627	0.253300011
H	0.000000000	0.000000000	0.500000000

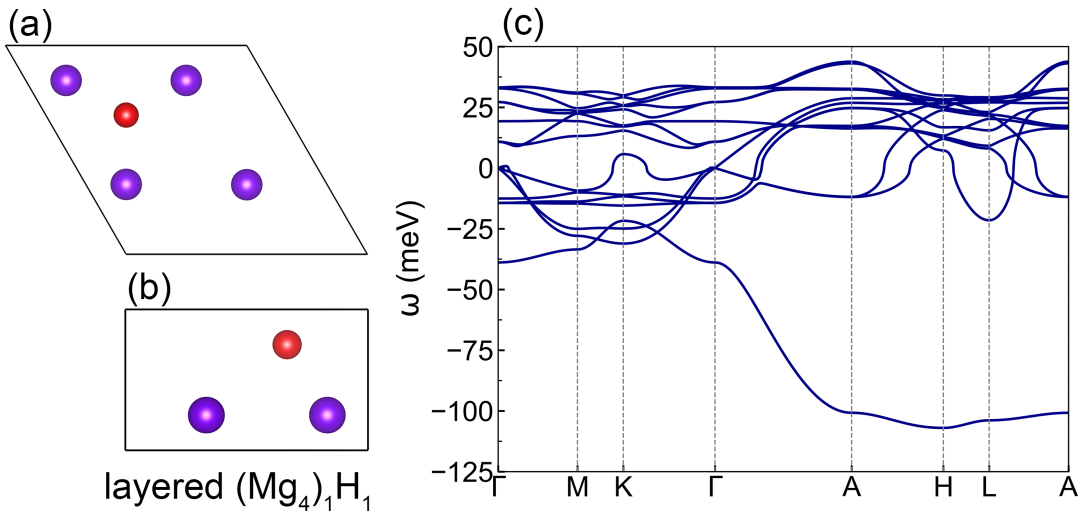

FIG. S2. (a) Top and (b) side views of layered $(Mg_4)_1H_1$. (c) Calculated phonon dispersions of $(Mg_4)_1H_1$. The imaginary frequencies clearly indicate that layered $(Mg_4)_1H_1$ is dynamically unstable at ambient pressure.

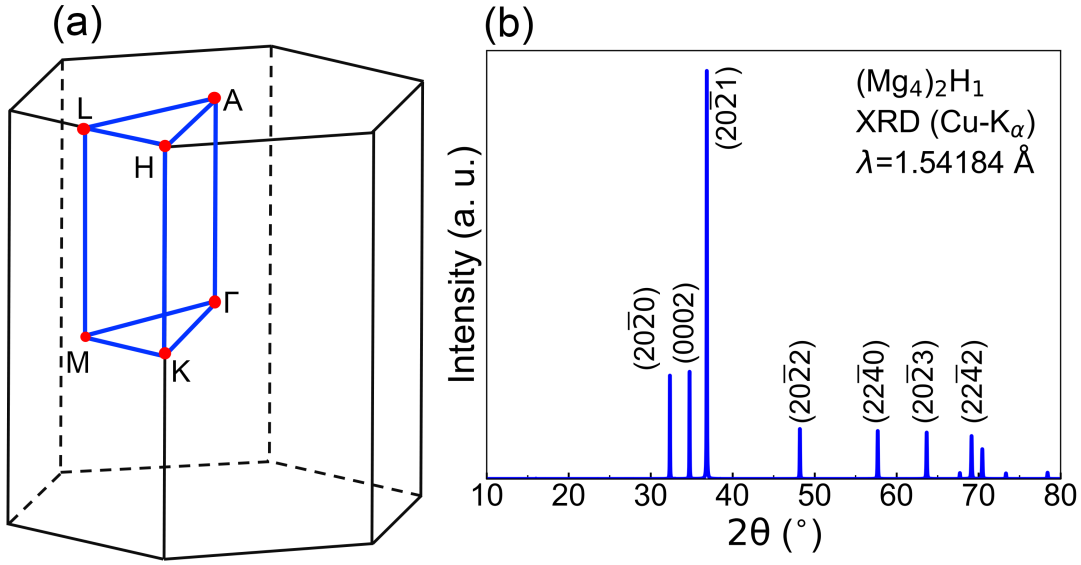

FIG. S3. (a) The first Brillouin zone of layered $(Mg_4)_2H_1$, where several high symmetry points are labeled by Γ, M, K, A, H and L, respectively. (b) The simulated X-ray diffraction (XRD) pattern for the optimized $(Mg_4)_2H_1$ from 10° to 80° by using the radiation wavelength λ=1.54184 Å (Cu-K_α). Several important peaks are marked with the corresponding Miller-Bravais indices.

ELECTRONIC STRUCTURE AND SUPERCONDUCTING PROPERTY

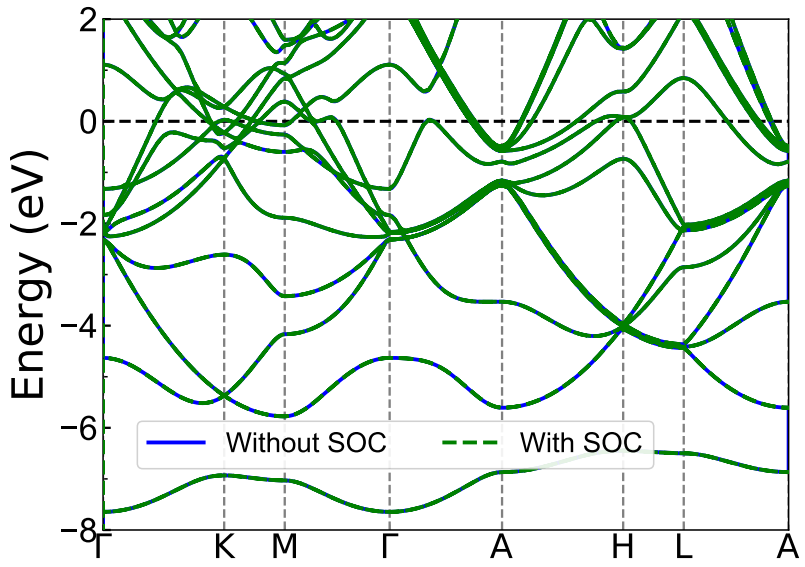

FIG. S4. The calculated band structure of layered $(Mg_4)_2H_1$. Here, the blue solid line and green dashed line represent the band structure without and with spin-orbit coupling (SOC), respectively. The completely coincident band structures demonstrate that the SOC effect can be neglected in our calculations.

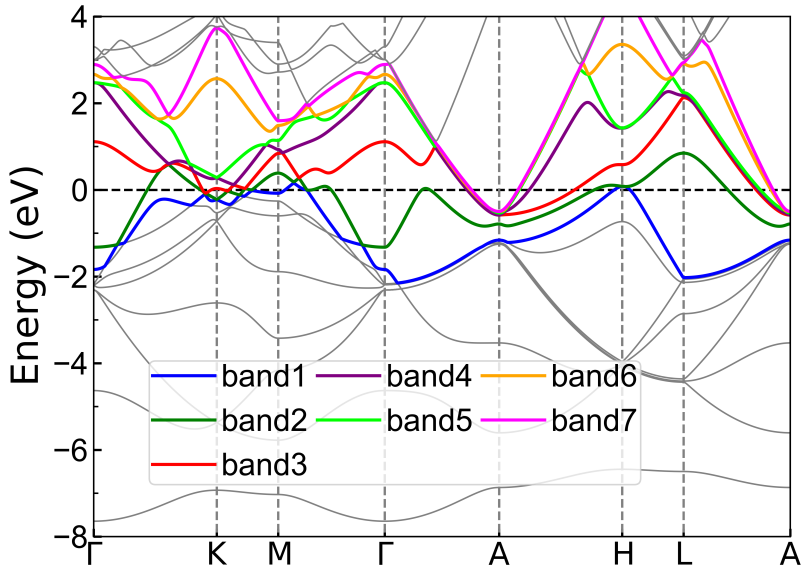

FIG. S5. The calculated band structure of layered $(Mg_4)_2H_1$ shows seven bands that cross the Fermi level, each labeled with a different color.

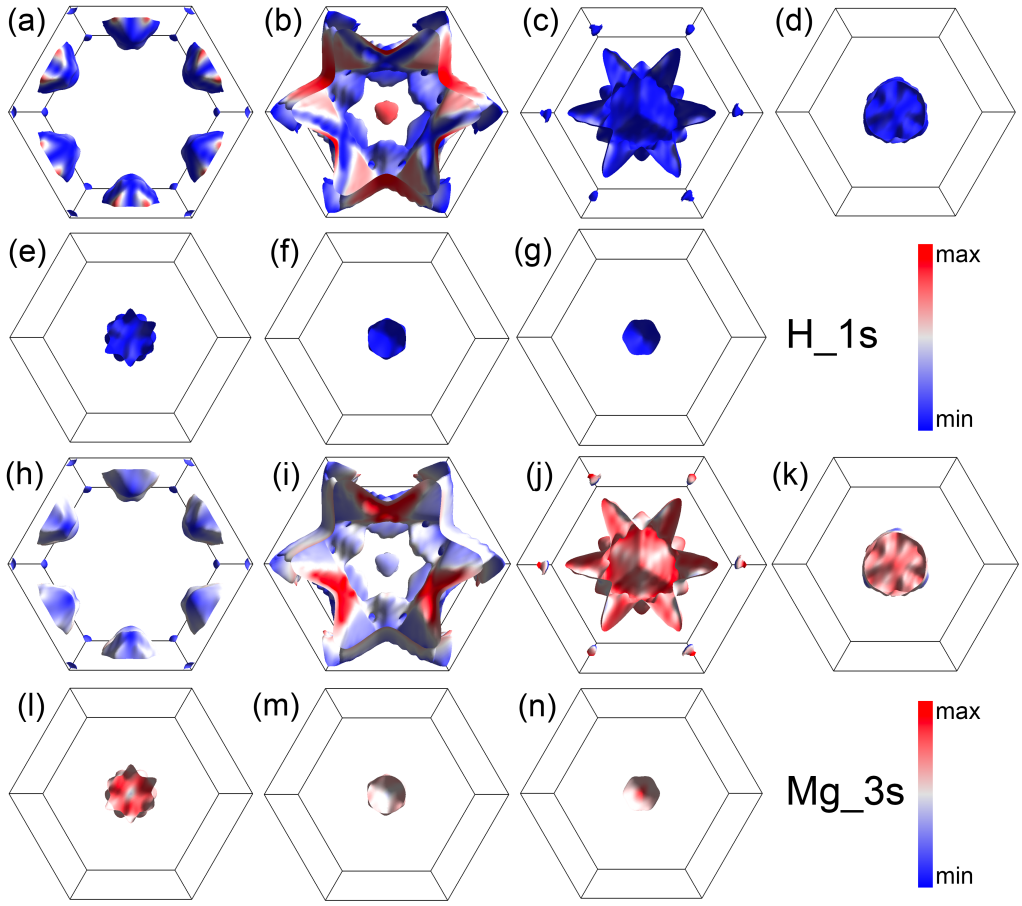

FIG. S6. Spectral weight on Fermi surface in layered $(Mg_4)_2H_1$. Spectral weight on Fermi surface for (a)-(g) H 1s orbital and (h)-(n) Mg 3s orbital.

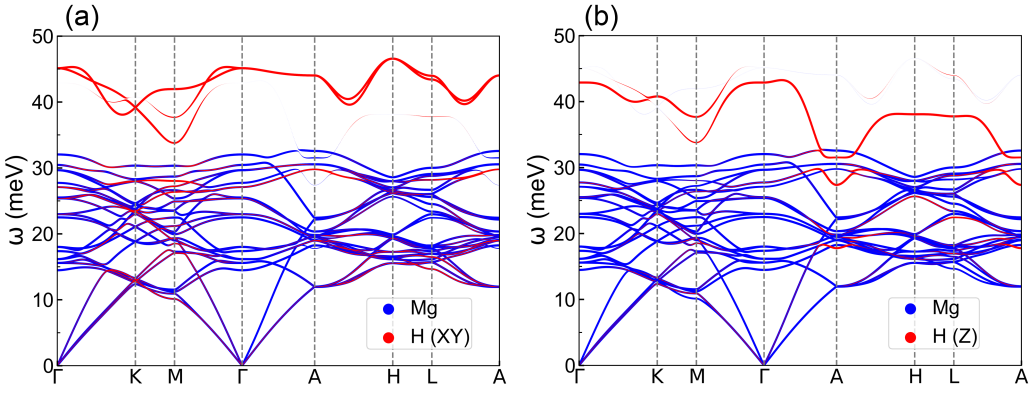

FIG. S7. (a) The calculated phonon dispersions for layered $(Mg_4)_2H_1$ are encoded in color, representing Mg vibrations and in-plane vibrations (xy direction) of H. (b) The phonon spectra are decorated with Mg vibrations and out-of-plane vibrations (z direction) of H.

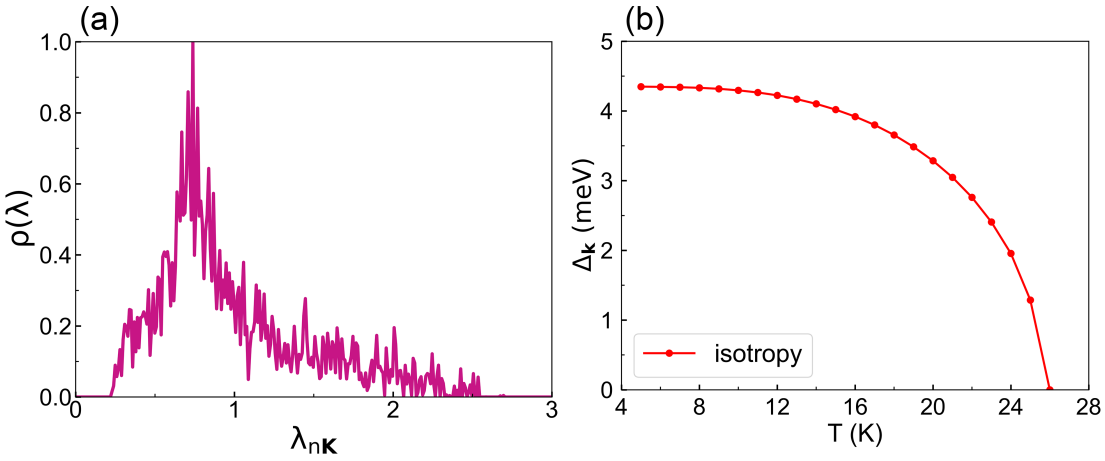

FIG. S8. (a) The normalized distribution of the EPC strength $\lambda_{n\mathbf{k}}$ in layered $(Mg_4)_2H_1$, revealing its strong anisotropy. (b) Calculated isotropic superconducting gap $\Delta_{\mathbf{k}}$ as a function of temperature, in which the semiempirical Coulomb repulsion pseudopotential μ^* is set to 0.10. The superconducting gap $\Delta_{\mathbf{k}}$ vanishes at superconducting transition temperature T_c=26 K.

[1] P. Giannozzi, S. Baroni, N. Bonini, M. Calandra, R. Car, C. Cavazzoni, D. Ceresoli, G. L. Chiarotti, M. Cococcioni, I. Dabo, A. D. Corso, S. de Gironcoli, S. Fabris, G. Fratesi, R. Gebauer, U. Gerstmann, C. Gougoussis, A. Kokalj, M. Lazzeri, L. Martin-Samos, N. Marzari, F. Mauri, R. Mazzarello, S. Paolini, A. Pasquarello, L. Paulatto, C. Sbraccia, S. Scandolo, G. Sclauzero, A. P. Seitsonen, A. Smogunov, P. Umari and R. M. Wentzcovitch, *J. Phys.: Condens. Matter*, 2009, **21**, 395502.

[2] P. Giannozzi, O. Andreussi, T. Brumme, O. Bunau, M. B. Nardelli, M. Calandra, R. Car, C. Cavazzoni, D. Ceresoli, M. Cococcioni, N. Colonna, I. Carnimeo, A. D. Corso, S. de Gironcoli, P. Delugas, R. A. DiStasio, A. Ferretti, A. Floris, G. Fratesi, G. Fugallo, R. Gebauer, U. Gerstmann, F. Giustino, T. Gorni, J. Jia, M. Kawamura, H.-Y. Ko, A. Kokalj, E. Küçükbenli, M. Lazzeri, M. Marsili, N. Marzari, F. Mauri, N. L. Nguyen, H.-V. Nguyen, A. O. de-la Roza, L. Paulatto, S. Poncé, D. Rocca, R. Sabatini, B. Santra, M. Schlipf, A. P. Seitsonen, A. Smogunov, I. Timrov, T. Thonhauser, P. Umari, N. Vast, X. Wu and S. Baroni, *J. Phys.: Condens. Matter*, 2017, **29**, 465901.

[3] P. Giannozzi, O. Baseggio, P. Bonfà, D. Brunato, R. Car, I. Carnimeo, C. Cavazzoni, S. de Gironcoli, P. Delugas, F. Ferrari Ruffino, A. Ferretti, N. Marzari, I. Timrov, A. Urru and S. Baroni, *J. Chem. Phys.*, 2020, **152**, 154105.

[4] J. P. Perdew, A. Ruzsinszky, G. I. Csonka, O. A. Vydrov, G. E. Scuseria, L. A. Constantin, X. Zhou and K. Burke, *Phys. Rev. Lett.*, 2008, **100**, 136406.

[5] J. P. Perdew, K. Burke and M. Ernzerhof, *Phys. Rev. Lett.*, 1996, **77**, 3865–3868.

[6] M. Schlipf and F. Gygi, *Comput. Phys. Commun.*, 2015, **196**, 36–44.

[7] S. Baroni, S. de Gironcoli, A. Dal Corso and P. Giannozzi, *Rev. Mod. Phys.*, 2001, **73**, 515–562.

[8] P. B. Allen and R. C. Dynes, *Phys. Rev. B*, 1975, **12**, 905–922.

[9] P. B. Allen, *Phys. Rev. B*, 1972, **6**, 2577–2579.

[10] P. B. Allen and B. Mitrović, *Solid State Phys.*, 1983, **37**, 1–92.

[11] E. R. Margine and F. Giustino, *Phys. Rev. B*, 2013, **87**, 024505.

[12] F. Giustino, M. L. Cohen and S. G. Louie, *Phys. Rev. B*, 2007, **76**, 165108.

[13] S. Poncé, E. R. Margine, C. Verdi and F. Giustino, *Comput. Phys. Commun.*, 2016, **209**, 116–133.

[14] F. Giustino, *Rev. Mod. Phys.*, 2017, **89**, 015003.

[15] G. Pizzi, V. Vitale, R. Arita, S. Blügel, F. Freimuth, G. Géranton, M. Gibertini, D. Gresch, C. Johnson, T. Koretsune, Y. Mokrousov, J. I. Mustafa, Y. Nohara, Y. Nomura, L. Paulatto, S. Poncé, T. Ponweiser, J. Qiao, F. Thöle, S. S. Tsirkin, M. Wierzbowska, N. Marzari, D. Vanderbilt, I. Souza, A. A. Mostofi and J. R. Yates, *J. Phys.: Condens. Matter*, 2020, **32**, 165902.

[16] J. Bardeen and M. Stephen, *Phys. Rev.*, 1964, **136**, A1485–A1487.

[17] H. J. Choi, M. L. Cohen and S. G. Louie, *Physica C*, 2003, **385**, 66–74.

[18] J. P. Carbotte, *Rev. Mod. Phys.*, 1990, **62**, 1027–1157.